AJNR Am J Neuroradiol 20:1907–1914, November/December 1999

MR Blood Oxygenation Level–Dependent Signal Differences in Parenchymal and Large Draining Vessels: Implications for Functional MR Imaging

Timo Krings, Stephan G. Erberich, Florian Roessler, Jürgen Reul, and Armin Thron

BACKGROUND AND PURPOSE: **One major limitation of current functional MR (fMR) imaging is its inability to clarify the relationship between sites of cortical neuronal activation, small parenchymal venules that are in close proximity to these sites, and large draining veins distant from the active parenchyma. We propose to use gradient-echo blood oxygenation level–dependent (BOLD) fMR time courses to differentiate large draining veins from parenchymal microvasculature.**

METHODS: **In eight research subjects, five of whom presented with space-occupying lesions near the central sulcus, gradient-echo fMR imaging was performed during alternating periods of rest and motor activation. MR signal time courses from parenchymal regions and draining veins of different diameters, which were identified using contrast-enhanced T1-weighted scans, were evaluated. Percent signal changes (ΔS) and the time to the onset of MR signal rise (T_0) were calculated.**

RESULTS: **Mean ΔS for all subjects was 2.3% (SD ±0.7%) for parenchymal activation, 4.3% (SD ±1.0%) for sulcal macrovasculature, and 7.3 (SD ±1.1%) for large superficial bridging veins. The mean time to onset of MR signal increase was 4.4 seconds for parenchymal task-related hemodynamic changes and 6.6 seconds for venous hemodynamic changes, regardless of vessel size. Both the differences in ΔS and T_0 were statistically significant between venous and parenchymal activation ($P < .0001$).**

CONCLUSION: **Gradient-echo fMR imaging reveals hemodynamic task-related changes regardless of vessel size and therefore might show macrovascular changes distal to the site of neuronal activity. MR-signal time-course characteristics (ΔS and T_0) can be used to differentiate between small parenchymal and larger pial draining vessels, which is especially important in presurgical planning of neurosurgical procedures involving functionally important brain regions. The knowledge about the differences in ΔS and T_0 between micro- and macrovasculature might lead to a more accurate description of the spatial distribution of underlying neuronal activity.**

Neuronal activity causes changes in CBF, cerebral blood volume (CBV), and blood oxygenation. It has been demonstrated that MR imaging can be used to detect these subtle cerebral hemodynamic changes with appropriate pulse sequences. Several studies have shown that these specifically designed sequences can be used for noninvasive mapping of human brain function. Functional MR (fMR) imaging techniques that investigate the various aspects of cerebral hemodynamics (CBV [1], CBF [2], and blood oxygenation) have been developed. Of these different MR techniques, blood oxygenation level dependent (BOLD) sequences are used most extensively.

BOLD functional MR imaging uses the intrinsic paramagnetic signal of deoxyhemoglobin (dHB) to depict local changes in blood flow associated with neuronal activity. During cognitive activation, regional CBF (and therefore the rate of oxygen delivery) has a proportionally higher increase than does local oxygen consumption, resulting in a decrease of paramagnetic dHB content in draining capillaries and veins (3, 4). Because dHB increases magnetic field strength, it creates intra- and perivascular field gradients, spin-phase coherence loss

Received November 9, 1998; accepted after revision June 14, 1999.

From the Department of Neuroradiology and the Interdisciplinary Center for Clinical Research—Central Nervous System, University Hospital of the Technical University, Aachen, Germany.

Address reprint requests to Timo Krings, MD, Department of Neuroradiology, University Hospital of the Technical University Aachen, Pauwelsstrasse 30, 52057 Aachen, Germany.

on T2*-weighted pulse sequences, and a consecutive attenuation of MR signal intensity (5, 6). Statistical correlation between the MR signal time course and the cognitive paradigm identifies those regions that demonstrate task-related changes in MR signal intensity (7).

One major limitation of functional MR imaging is the still unknown relationship between the localization of the depicted task-related hemodynamic changes and the cortical area of neuronal activity (8–10). This so-called ''brain or vein'' problem (11) describes the lack of knowledge about whether or not large draining veins, which have no close relationship to the areas of cerebral activation or small parenchymal venules in close proximity to the sites of neuronal activity, are depicted during BOLD functional MR imaging. This problem becomes especially important if functional MR imaging results are used for presurgical mapping of functional cortical areas in relationship to underlying brain lesions. To date, the most common approach used to differentiate between large draining veins and small parenchymal veins has been the visual inspection of the functional MR imaging activation pattern in correlation with anatomic images (12). More elaborate studies have correlated their activation patterns to venous angiograms (13) or have cross-validated their sequences with other electrophysiologically and hemodynamically based mapping techniques, including positron-emission tomography (14), direct electrical cortical stimulation (15), magnetoencephalography (16), electroencephalography (17), or transcranial magnetic stimulation (18). Instead of these cross-validation techniques, the aim of the present study was to use MR-signal time-course characteristics in a typical fMR imaging experiment to differentiate between small parenchymal venules and large draining veins that are demonstrated by contrast-enhanced T1-weighted studies.

Methods

Eight subjects (23–65 years old), of whom five underwent presurgical evaluation for tumors in the area of the central sulcus, were investigated. All experiments were performed on a clinical 1.5-T scanner equipped with echo-planar imaging (EPI) capabilities (Gyroscan ACS NT, Philips Medical Systems, Best, the Netherlands). The subjects were rigidly fixated in a standard headcoil by using Velcro straps and foam padding to minimize motion artifacts. For each subject before each scan was obtained, field homogeneity was optimized using an automatic shimming sequence.

Anatomic Images

Six contiguous T1-weighted spin-echo slices were obtained for anatomic reference and were oriented parallel to the line running through the anterior and the posterior commissure. Images were obtained solely from the suprasylvian region (100/14 [TR/TE]; flip angle, 90°; matrix, 256 × 256; field of view, 250 × 175 mm; and slice thickness, 5 mm). After the functional scans were performed, this T1-weighted anatomic sequence was repeated after administration of Gd-DTPA. At the end of the scanning procedure, a 3D phase-contrast gradient-echo (GE) angiographic sequence (20/8.6 [TR/TE]; flip angle, 15°; matrix, 256 × 256; flow selectivity, 10 mm/s) was obtained. Each scan (anatomic, functional, postcontrast, angiographic) was obtained with the same slice number, orientation, and localization.

Functional Images

BOLD imaging was performed on all eight subjects using a multi-shot T2*-weighted GE EPI sequence (278/35 [TR/TE]; flip angle, 35°; matrix, 64 × 64; field of view, 250 × 175 mm). Six 5-mm-thick slices were obtained that had the same localization and orientation as the anatomic slices. One hundred two images were generated (2.2 s/image) during a total imaging time of 3 minutes 42 seconds.

Each task paradigm consisted of six 37-second blocks alternating between rest and activation. The specific task was the repetitive, self-paced opening and closing of the hand (''hand clenching''). The activity was performed with a frequency of approximately 1 Hz. Hand clenching was used as opposed to finger tapping because it constitutes a simpler movement requiring less fine-motor activity, which was impaired in some patients with tumors near the central sulcus. One additional subject was investigated with a faster sequence employing only two 5-mm-thick slices. This faster sequence focused on the paracentral lobule, which enabled a temporal resolution of 556 ms/image.

Each subject repeated the functional task twice. In one patient, only one study was performed because of the patient's discomfort in the scanner. Subjects gave written informed consent for participation in the study. None of the subjects experienced any procedure-related side effects.

To minimize the effects of interimage motion-related artifacts, we employed an automated image realignment algorithm for each set of functional data (19). Sites of functional activation were identified on a voxel by voxel basis using the Kolmogorov Smirnov nonparametric statistical test to compare the MR signal time course with the given task paradigm. Activation maps were color-coded according to the statistical significance of difference between the rest and activation states and overlaid upon the anatomic T1-weighted images, the venous angiograms, and the contrast-enhanced T1-weighted images for anatomic reference and detection of venous structures. Task-related MR signal changes arising from draining veins could be identified reliably by toggling the activation maps over the contrast-enhanced scans.

During signal time-course analysis, the following steps were performed independently for ''activated'' regions overlaying the parenchyma, small veins in the depth of the central sulcus, and large veins on the cortical surface parenchyma. First, percent signal change (ΔS), and then determination of the latency between onset of task activity and onset of signal rise time (T_0) were calculated. To minimize partial volume effects, only one voxel for each region was evaluated. We selected this voxel according to its statistical power. Percent signal change was calculated between the arithmetic mean MR signal-intensity baseline value and the mean MR signal-intensity activated-state value. The time of onset of MR signal-intensity rise was determined as follows. The standard deviation for the baseline MR signal-intensity values was calculated. The time of onset (T_0) was defined as the first time-point after task initiation in which the MR signal intensity was consistently (five consecutive time-points) higher than the mean baseline plus twice the standard deviation. To test for intrasubject variation of ΔS, the arithmetic error between the two functional runs was calculated.

A two-tailed paired Student *t*-test was performed to determine whether there were any statistically significant differences in ΔS and T_0 between parenchymal and venous ''activation'' or between large superficial veins and small sulcal veins, ignoring the fact that repeated pairs of measurement of the same subject might be positively correlated.

MR BOLD signal characteristics for veins of different sizes*

	S1	S2	S3	S4	S5	S6	S7**	S8	MEAN (+SD)
Parenchyma									
Baseline S (abs)	882	921	1008	933	917	914	877 *893*	974	924 (±43)
Baseline N (%)	1.9	1.0	1.2	1.6	2.1	1.4	1.8 *1.4*	1.5	1.5 (±0.4)
ΔS (%)	2.4	3.1	1.8	1.5	3.6	2.0	1.9 *1.4*	2.3	2.3 (±0.7)
Mean T_o (sec)	4.6	3.7	4.0	***	4.4	3.7	4.8 *4.6*	3.3	4.2 (±1.3)
Range T_o (sec)	2.2–6.6	2.2–4.4	2.2–4.4	***	2.2–6.6	2.2–4.4	2.2–6.6	2.2–4.4	
Sulcal Vein									
Baseline S (abs)	824	816	923	778	891	845	767 *744*	845	825 (±58)
Baseline N (%)	1.4	1.3	2.4	1.9	1.8	1.1	1.0 *1.4*	1.9	1.6 (±0.4)
ΔS (%)	5.1	4.9	3.9	3.6	5.8	4.1	3.4 *4.6*	4.1	4.3 (±1.0)
Mean T_o (sec)	5.1	7.0	6.6	6.6	7.0	7.3	6.6 *6.6*	5.5	6.4 (±2.0)
Range T_o (sec)	4.4–6.6	4.4–8.8	2.2–8.8	4.4–8.8	4.4–8.8	4.4–8.8	4.4–8.8	2.2–8.8	
Bridging Vein									
Baseline S (abs)	751	789	714	812	729	707	828 *833*	843	778 (±54)
Baseline N (%)	1.8	1.4	1.8	1.2	1.8	1.3	1.4 *1.4*	2.2	1.6 (±0.3)
ΔS (%)	8.4	8.7	6.9	6.9	6.9	8.0	5.9 *6.0*	6.8	7.3 (±1.1)
Mean T_o (sec)	5.9	7.0	7.0	7.0	6.2	7.0	6.2 *6.6*	6.0	6.6 (±1.3)
Range T_o (sec)	4.4–8.8	6.6–8.8	4.4–8.8	6.6–8.8	4.4–8.8	4.4–8.8	4.4–8.8	4.4–8.8	

Note.—Baseline S, mean baseline signal in absolute values; Baseline N, mean percent signal noise; ΔS, mean percent gradient–echo BOLD MR signal changes; Mean $T_{o,}$ mean time delay until a significant increase from the baseline (mean value + 2SD) is noted; Range T_o range of onset times using a time resolution of 2.2 sec per scan.

* All values represent the mean of two functional runs performed during the same imaging session.

** In subject 7, two imaging sessions consisting of two functional runs were performed 10 days apart. The values for the latter session are given in italics.

*** In subject 4 no significant increase from the baseline was noted.

Results

Motor activation induced robust task-related hemodynamic changes in the primary sensorimotor cortex contralateral to the activated hand in all of the investigated subjects. The pattern of activation was similar in all subjects: deep medial activity located in the ''hand knob'' (20), an omega-shaped part of the precentral gyrus, and, typically in the same slice, more superficial lateral activity within the central sulcus. In subsequent higher slices, the lateral activation still was visible on the superficial cortex, whereas the medial activity was maximally located on two subsequent slices. The lateral activity always was contiguous on the adjacent slices in all investigated subjects, extended toward the superior sagittal sinus, and had a tubular structure, presumably corresponding to the central sulcal vein.

The area of activation on the surface of the brain, which was visible on multiple slices, was identified as a large draining vessel when overlaying the functional maps on the contrast-enhanced T1-weighted scan. The dual activation visible on at least one slice in each patient could be differentiated further when being merged with the venous anatomy. The lateral, more superficial area of activation co-localized in all cases in which a vessel was seen after administration of Gd-DTPA; however, the medial deep activation did not spatially coincide with a macrovessel.

Student *t*-test statistics of the time-course analysis revealed highly significant ($P < .0001$) differences in T_0 and ΔS between parenchymal and venous sites of task-related hemodynamic changes and highly significant differences in ΔS for superficial and sulcal veins. T_0 differences between superficial and sulcal veins were not significant. There were no significant differences in MR signal time-course characteristics between different runs in the same subject; ΔS demonstrated a mean percent signal change variation of 0.4% (range 0–1.7 %) between two different runs of the same subject. The Table herein shows the mean ΔS and T_0 values for all subjects. Mean ΔS for all subjects was 2.3% (SD ±0.7%) for parenchymal activation, 4.3% (SD ±1.0%) for sulcal macrovasculature, and 7.3% (SD ±1.1%) for large superficial bridging veins. The median time to onset of MR signal increase was 4.4 seconds for parenchymal task-related hemodynamic changes and 6.6 seconds for venous hemodynamic changes, regardless of vessel size. In all but one functional run (subject 1, run 2), there was no overlap in values between parenchymal and nonparenchymal T_0.

Figure 1 demonstrates signal time-course characteristics of parenchymal venules, sulcal veins, and superficial draining veins for two subsequent functional runs. Figure 2 demonstrates signal time-course characteristics overlaid on the T1-weighted postcontrast study for anatomic reference. Two phase-contrast (PC) MR angiographs with different flow sensitivities are shown adjacent to the functional activation.

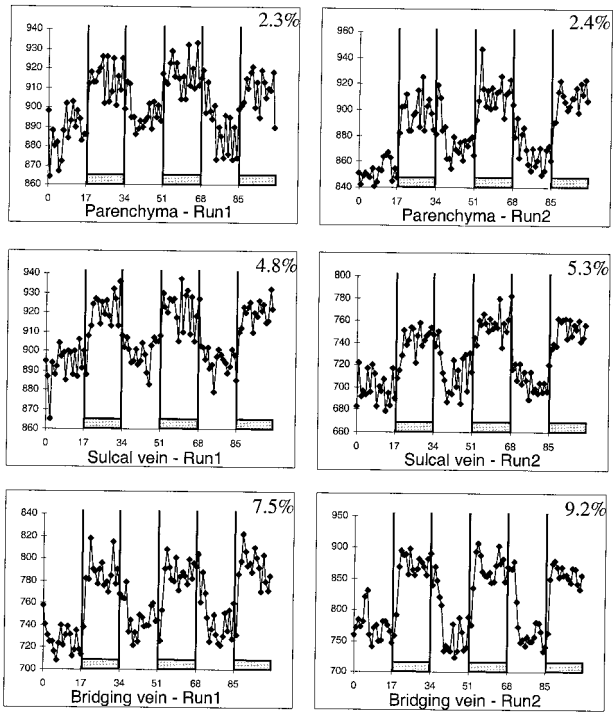

FIG 1. MR signal time courses for parenchyma, sulcal veins, and bridging veins for single subject in two different functional runs (hand clenching) (S1). Each diamond represents MR signal at one time-point. Temporal resolution of the sequence was 2.2 s/image. Mean percent signal changes increase as a function of vessel size. Note low test-retest variability of percent signal changes within the same subject.

The single subject who was investigated using a higher temporal resolution had similar ΔS values compared with the other eight subjects (parenchyma, 2.2% ΔS; sulcal vein, 3.1% ΔS; bridging vein, 5.7% ΔS). When evaluating the signal time-course, however, a finer temporal discrimination was possible. The first significant increases from baseline were noted in parenchymal venules (3A [3.4–3.9 seconds]), sulcal veins (3B [5.5–6.1 seconds]), and large bridging veins (3C [6.1–6.7 seconds]) after the subject moved his hand.

Illustrative Case

Patient 7 (28-year-old woman) underwent presurgical planning for a space-occupying lesion of unknown etiology near the central sulcus. Functional MR imaging showed dual activation in close proximity to the tumor in the central region. The lateral activity had a mean percent signal change of 3.4% and a T_0 of 6.6 seconds, whereas the respective values for the medial activity were ΔS 1.9% with a T_0 of 4.8 seconds. The medial activity showed posterior displacement, with the tumor directly anterior to the functional activation, whereas the stronger activity was displaced lateral to the tumor and at an in-plane distance of 3 mm to the medial activation. A stereotactic biopsy was taken after which the patient suffered from a paresis of the right small hand muscles with a loss of fine motor skills. An fMR imaging re-examination was performed 10 days after the first and 8 days after the biopsy was taken. The persistent paresis still allowed for hand clenching, with a marked decrease in finger movement rate compared with the initial functional MR imaging investigation. Anatomic images showed that the biopsy was taken from the posterior part of the lesion and also affected healthy tissue in which part of the medial activation of the former functional examination was seen. Subsequent activation maps again revealed dual activation with the lateral area unchanged in location, extent, percent signal change, and statistical significance, whereas the medial area showed more lateral displacement, directly adjacent to the biopsy site and decreased in extent, percent signal change, and peak statistical significance (Fig 4).

Discussion

Using the following criteria, merging of functional images with T1-weighted images can assist in the differentiation between functional MR signal changes of large draining vessels and those of small parenchymal vessels. Small parenchymal microvessels are represented by those voxels that are located mainly in the part of the gray matter that corresponds to functional anatomy (ie, hand knob) (20) and that do not extend to the superior surface of the brain where the major draining veins are located. This microvasculature has a close spatial relationship to the cortical sites of neuronal activation (12). Sulcal or superficial activity, on the contrary, presumably reflects large draining vessels such as bridging veins.

On contrast-enhanced T1-weighted images, additional pial vessels such as deep sulcal veins can be visualized. Merging of functional maps with these contrast-enhanced scans allows for an even finer differentiation of the size of the vasculature from which the functional MR signal change stems (13). Thus, we used morphologic, not physiologic, criteria to segment the observed signal changes. In the following, the term *microvasculature* will be used for those draining veins that show functional MR signal change during activation but are not visible on contrast-enhanced T1-weighted sequences nor do they follow the above-mentioned criteria for parenchymal vessels. The term *macrovasculature* will be used for those draining veins that can be seen on contrast-enhanced T1-weighted scans.

We have demonstrated both different localization and different signal time-course characteristics for macro- and microvasculature. We have observed dual activation in the central region after hand clenching in all subjects: a deep medial area reflecting parenchymal microvasculature and a more superficial lateral area reflecting pial macrovasculature. It is known from the venous anatomy of the pre- and postcentral gyrus that the central sulcus is filled with pial vessels draining from both banks of the central sulcus, with the larger veins primarily

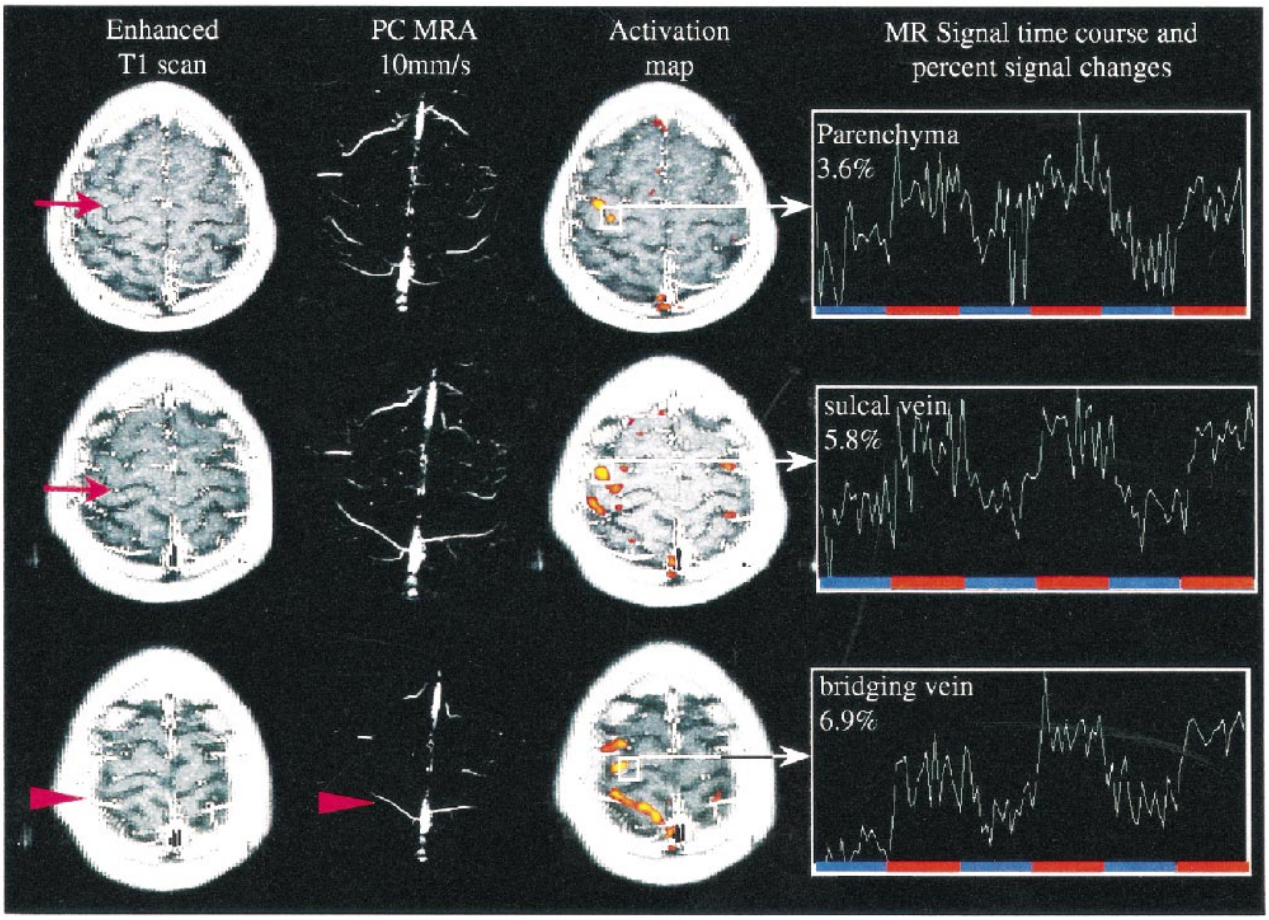

FIG 2. MR signal time course correlation with contrast-enhanced T1-weighted scans and phase-contrast MR angiography (S5). Contrast-enhanced studies reliably show sulcal and superficial veins, whereas the phase-contrast MR angiography with given flow sensitivity demonstrates vessels the size of large bridging veins. Significant change in MR signal (ΔS) is seen in bridging veins even close to superior sagittal sinus. From this data, one can presume that dilution of increased oxyhemoglobin content and therefore decay of ΔS takes place when bridging veins enter large draining sinuses. *Arrows* point at sulcal veins, *arrowheads* at large bridging veins.

draining upward, or in axial slices, draining laterally, toward the brain surface (21). The small venules of the parenchyma are in close spatial relationship to the activated neuronal tissue, maximally 1.5-mm apart and too small to be detectable on contrast-enhanced studies (22). Nonetheless, the larger sulcal veins, which are fed by smaller veins within the posterior and anterior banks of the pre- and postcentral gyri, respectively, are visible on contrast-enhanced studies. The lateral area of activation typically overlaid a vein visible on contrast-enhanced T1-weighted sequences, whereas the medial area did not. The lateral area extended over multiple slices and therefore had a tubular structure, most likely resembling a superficial draining vein. The fact that both micro- and macrovasculature are depicted by GE fMR imaging is further confounded by Monte-Carlo modeling of susceptibility physics. Unlike spin-echo sequences, GE sequences are not specific in the detection of vessel sizes (23–25). Spin-echo sequences, on the contrary, have a high specificity for microvessels but are less sensitive to magnetic susceptibility effects. At 1.5 T, functional contrast for both sequences is quite similar within parenchymal regions, whereas signal changes in large vessels is reduced greatly by employing an additional refocusing pulse as used in spin-echo sequences (26). This diminution of signal arising from large vessels is not observed with GE sequences. The decreased specificity for detected vessel size of GE sequences is traded against a higher overall sensitivity for magnetic susceptibility differences and, therefore, a higher percent signal change in GE sequences compared with spin-echo sequences. Most fMR imaging studies employ GE sequences for this reason.

We have found a considerably higher ΔS in macrovessels compared with parenchymal microvessels, which was reported also by Kim et al (9) and Gati et al (27). These differences of percent BOLD MR signal intensity changes observed in the described GE pulse sequence can be explained by different effects. First, Monte-Carlo modeling of susceptibility contrast physics has shown that the intravascular contribution of venules and veins to the T2*-weighted signal change exceeds that of capillaries. Therefore, GE sequences yield a considerably higher signal in macrovessels compared

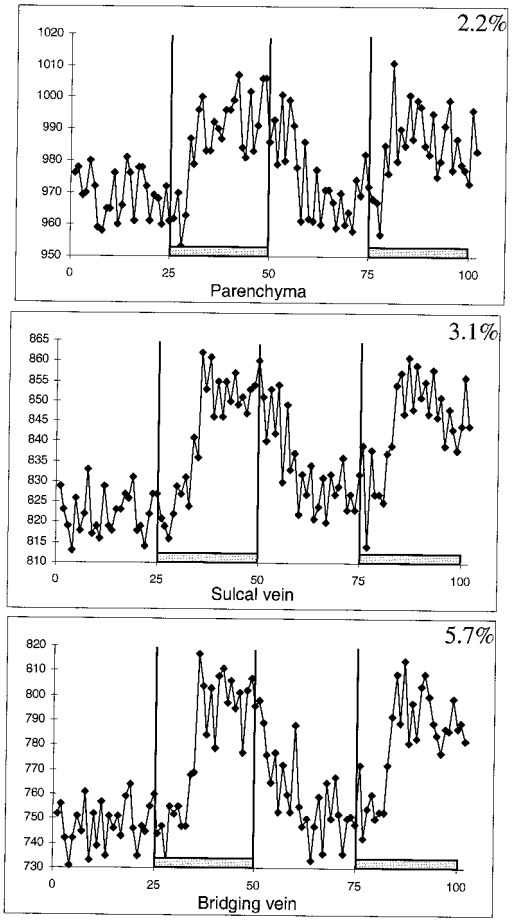

FIG 3. MR signal time courses for parenchyma, sulcal veins, and bridging veins for subject scanned with higher temporal resolution (556 ms/image) during hand clenching. With a finer temporal resolution, the differences in onset of significant task related MR signal changes between vessels of different diameter can be visualized.

with microvessels (23–25). In addition, in vivo measurements have shown that the region that contributes the intravoxel dephasing extends as far as twice the vessel diameter (5). This means that the volume that contributes to the dephasing is four times that of the vessel volume if one treats a cylinder as a two-dimensional object (5). Therefore, magnetic susceptibility effects and a concomitant increase in ΔS are enhanced presumably around large veins draining an extended activated region (12). The macroscopic signal increase during neuronal activation reflects a net increase in brain oxygenation within extended-field brain tissue. A second explanation for the more prominent increase in ΔS in larger vessels is, therefore, partial volume effect. Because parenchymal vessels are considerably smaller than are the draining macrovessels, parenchymal activation suffers from larger partial volume averaging, with brain tissue unaffected by the motor activation. The corresponding diminution of the mean signal change theoretically could be removed by reducing the slice thickness and increasing the imaging matrix, because it is known that object contrast and visibility increase as resolution increases until the voxel size is similar to the object size (28). A third explanation is inflow effects, which have a significant impact on percent signal changes (8, 10) and are more pronounced in large vessels than in cortical microvasculature. It is known from studies of the structure of the microvasculature within the brain that there is a random distribution of capillary orientation (29). Inflow effects are of particular interest in functional neuroimaging when large flip angles, thin slices, and short TRs are used. The fourth explanation is that ΔS also might be higher in the macrovasculature, because the venous drainage in larger sulcal vessels might have contributions from a larger area. It is known from the venous anatomy of the pre- and postcentral gyrus that the central sulcus is filled with pial vessels draining from both banks of the central sulcus (21). During motor tasks, both the precentral gyrus and the postcentral sensory cortex are active, presumably because of sensory feedback during the performance of the motor task (13). Draining veins in the central sulcus and the cortical surface collect from a larger area of cortex and, therefore, demonstrate enhanced hemodynamic changes. As Malonek and Grinvald indicated (30, 31), this increased inflow is regulated at a rather coarse spatial scale.

Differences in the onset of signal change between large draining veins and cortical microvasculature have been reported previously (32). It was shown that signals from large vessels are time-delayed compared with those from small vessels. The larger delay is consistent with the longer time required for blood to reach larger vessels. We were able to demonstrate similar MR signal time-course characteristics. Our time resolution was rather coarse (2.2 s/scan), yet the differences in T_0 were statistically significant between venous and parenchymal ''activation.'' There, however, was no significant difference between the larger draining veins (ie, sulcal and superficial bridging veins). These results were confirmed in the single subject who was examined with a higher temporal resolution. The earlier onset in the microvasculature reflects hemodynamic changes in draining vessels that are more closely time-locked to the neuronal activation and, therefore, demonstrate a better spatial concordance to the site of neuronal activity. In contrast to ΔS, which only reflects vessel size, T_0 seems to reflect the vascular transit time from the capillary bed to the large draining veins.

Caution must be exercised when evaluating higher cortical functions such as language or when performing neuropsychological studies using GE functional MR imaging. In these studies, the more widespread area of activation, the more distributed neuronal activity, and the differences in the structure of the cortical microcirculation yield relatively lower percent signal changes (typically up to 2%). Given a background noise of approximately 1.5%, this parenchymal percent signal change might be

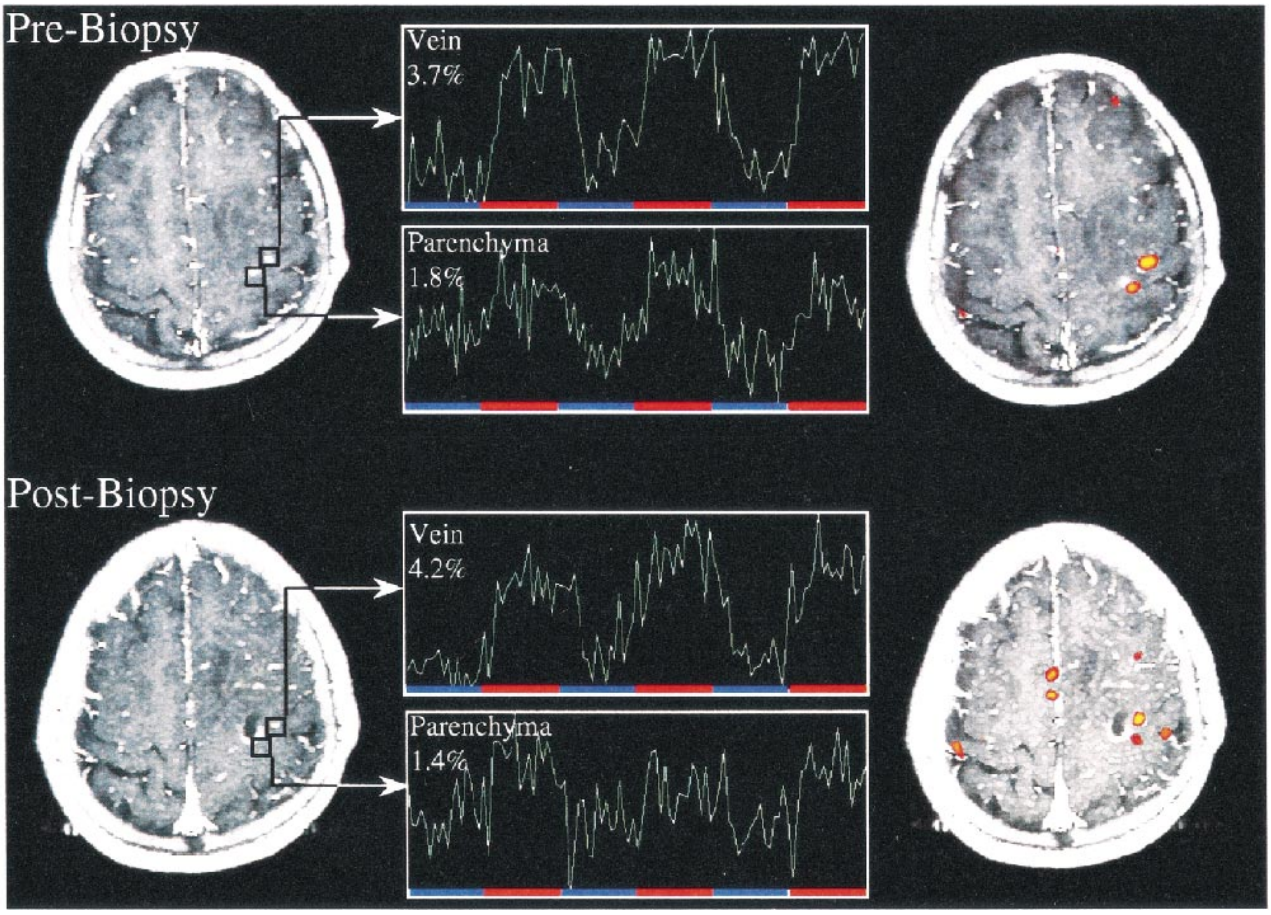

FIG 4. Functional MR and MR signal time course. This patient was evaluated for presurgical planning of a space-occupying lesion near central sulcus (Astrocytoma III) (S7). The first fMR imaging study shows dual activation in slice of interest with parenchymal activation located in close proximity to tumor. A stereotactic biopsy was performed after which the patient suffered from transient mild paresis of the small right hand muscles. A postbiopsy MR image demonstrates that the biopsy involved a previously activated region posterior to the lesion. Functional study again shows dual activation with parenchymal activation close to biopsy tract and lateral venous activity unaffected by biopsy. This case illustrates the importance of differentiating task-related hemodynamic changes of small parenchymal venules and large draining veins.

too low to yield statistically significant results (7). In these cases, parenchymal activation with a lower statistical power might not be detectable, whereas venous activation is, which leads to misinterpretation of the anatomic correlate of the specific task-related activity, because only larger venous structures demonstrate a high enough ΔS and, therefore, a high enough statistical power. Coregistration of functional maps with contrast-enhanced T1-weighted images might help in these studies to subtract signal arising from the macrovasculature. A second approach is to use the described differences in T_0 and ΔS to discern micro- from macrovasculature. Preliminary work from our group has shown that it is possible to use an unsupervised self-organizing-map neural-network technique that separates the voxels in the time-domain into different clusters. This technique might result in an automated detection and corrective algorithm for venous structures (33). A third approach is to increase the overall signal and, therefore, the ability to detect subtle signal changes in gray matter by using higher field strengths of the scanner. Because the absolute value of volume susceptibility differences between oxygenated and deoxygenated hemoglobin is more pronounced at high field strength (34), higher field imaging magnets increase the observed T2* changes (9, 27).

Conclusion

Because fMR imaging depicts hemodynamic changes in the human brain, it is of concern that larger vessels downstream from the actual site of neuronal activation are depicted instead of neuronal tissue. We have demonstrated that the GE BOLD MR signal changes in macrovessels are larger than in microvessels. This is important when evaluating studies for which exact localization of functional areas is paramount (ie, presurgical mapping) and for studies with a low signal-to-noise ratio (ie, studies of higher cognitive functions). GE functional MR imaging might show only hemodynamic changes within the macrovasculature distant from the site of neuronal activity. Although the values presented herein represent only one GE sequence,

it is not obvious why different GE sequences should yield significantly different results. Variation of MR imaging parameters will definitely enhance or diminish percent signal change. Geometric imaging parameters such as matrix size and slice thickness will lead to an increased ΔS if resolution is enhanced, lowering the possibility for unwanted partial volume effects; slice thicknesses of > 8 mm will suffer from considerable partial volume averaging with concomitant signal decrease (35). The choice of echo time also will have a considerable effect on signal intensity and observed signal changes. Even though susceptibility weighting is increasing at longer echo times, the measurable signal strength will decrease because of system instabilities, imaging artifacts, and, of course, T2 relaxation processes (35, 36). These changes, however, are not likely to affect the relative differences between parenchymal and sulcal activation, which, therefore, might be used to differentiate the fMR signal.

References

1. Belliveau JW, Kennedy DN, McKinstry RC, et al. **Functional mapping of the human visual cortex by magnetic resonance imaging.** *Science* 1991;254:716–719
2. Kwong KK, Bellieveau JW, Chesler DA, et al. **Dynamic magnetic resonance imaging of human brain activity during primary sensory stimulation.** *Proc Natl Acad Sci USA* 1992;89:5675–5679
3. Fox PT, Raichle ME. **Focal physiological uncoupling of cerebral blood flow and oxidative metabolism during somatosensory stimulation in human subjects.** *Proc Natl Acad Sci USA* 1986; 83:1140–1144
4. Fox PT, Raichle ME, Mintun MA, Dence C. **Nonoxidative glucose consumption during focal physiologic neural activity.** *Science* 1988;241:462–464
5. Ogawa S, Lee TM, Nayak AS, Glynn P. **Oxygenation-sensitive contrast in magnetic resonance image of rodent brain at high magnetic fields.** *Magn Reson Med* 1990;14:68–78
6. Turner R, Le Bihan D, Moonen CT, Despres D, Frank J. **Echo-planar time course MRI of cat brain oxygenation changes.** *Magn Reson Med* 1991;22:159–166
7. Kwong KK. **Functional MRI with echo planar imaging.** *Magn Reson Q* 1995;11:1–20
8. Duyn JH, Moonen CTW, van Yperen GH, de Boer RW, Luyten PR. **Inflow versus deoxyhemoglobin effects in BOLD functional MRI using gradient echoes at 1.5T.** *NMR Biomed* 1994;7:83–88
9. Kim SG, Hendrich K, Hu X, Merkle H, Ugurbil K. **Potential pitfalls of functional MRI using conventional gradient recalled echo techniques.** *NMR Biomed* 1994;7:69–74
10. Righini A, Pierpaoli C, Barnett AS, Waks E, Alger JR. **Blue blood or black blood: R1 effects in gradient-echo echo-planar functional neuroimaging.** *Magn Reson Imaging* 1995;13:369–378
11. Frahm J, Merboldt KD, Hänicke W, Kleinschmidt A, Böcker H. **Brain or vein—oxygenation or flow? On signal physiology in functional MRI of human brain activation.** *NMR Biomed* 1994; 7:45–53
12. Van Gelderen P, Ramsey NF, Liu G, et al. **Three-dimensional functional magnetic resonance imaging of human brain on a clinical 1.5-T scanner.** *Proc Natl Acad Sci* 1995;92:6906–6910
13. Krings T, Reul J, Spetzger U, Klusmann A, Roessler F, Gilsbach JM, et al. **Functional magnetic resonance mapping of sensory motor cortex for image-guided neurosurgical intervention.** *Acta neurochirurgica* 1998;140:215–222
14. Kraut MA, Marenco S, Soher BJ, Wong DF, Bryan RN. **Comparison of functional MR and $H_2{}^{15}O$ positron emission tomography in stimulation of the primary visual cortex.** *AJNR Am J Neuroradiol* 1995;16:2101–2107
15. Jack CR, Thompson RM, Butts RK, et al. **Sensory motor cortex: correlation of presurgical mapping with functional MR imaging and invasive cortical mapping.** *Neuroradiology* 1994;190: 85–92
16. Beisteiner R, Comiscek G, Erdler M, Teichtmeister C, Moser E, Deeke L. **Comparing localization of conventional functional magnetic resonance imaging and magnetoencephalography.** *Eur J Neurosci* 1995;7:1121–1124
17. Grimm C, Schreiber A, Kristeva-Feige R, Mergner T, Hennig J, Lücking CH. **A comparison between electric source localization and fMRI during somatosensory stimulation.** *Electroenceph Clin Neurophysiol* 1998;106:22–29
18. Krings T, Buchbinder BR, Butler WE, et al. **Functional magnetic resonance imaging and transcranial magnetic stimulation: Complementary approaches in the evaluation of cortical motor function.** *Neurology* 1997;48:1406–1416
19. Friston KJ, Ashburner J, Frith CD, Poline JB, Heather JD, Frackowiak RSJ. **Spatial registration and normalization of images.** *Human Brain Mapping* 1995;3:165–189
20. Yousry TA, Schmid UD, Alkahdi H, et al. **Localization of the motor hand area to a knob on the precentral gyrus. A new landmark.** *Brain* 1997;120:141–157
21. Duvernoy HM, Delon S, Vannson JL. **Cortical blood vessels of the human brain.** *Brain Res Bull* 1981;7:519–579
22. Lai S, Hopkins AL, Haacke EM, et al. **Identification of vascular structures as a major source of signal contrast in high resolution 2D and 3D functional activation imaging of motor cortex at 1.5T: Preliminary results.** *Magn Reson Med* 1993; 30:387–392
23. Weisskoff RM, Zuo C, Boxerman JL, Rosen BR. **Microscopic susceptibility variation and transverse relaxation: theory and experiment.** *Magn Reson Med* 1994;31:601–610
24. Boxerman JL, Bandettini PA, Kwong KK, et al. **The intravascular contribution of fMRI signal change: Monte Carlo modeling and diffusion-weighted studies in vivo.** *Magn Reson Med* 1995;34:4–10
25. Boxerman JL, Hamberg LM, Rosen BR, Weisskoff RM. **MR contrast due to intravascular magnetic susceptibility perturbations.** *Magn Reson Med* 1995;34:555–566
26. Buchbinder BR, Cosgrove GR. **Cortical activation MR studies in brain disorders.** *MRI Clin North Am* 1998;6:67–93
27. Gati JS, Menon RS, Ugurbil K, Rutt BK. **Experimental determination of the BOLD field strength dependence in vessels and tissue** *Magn Reson Med* 1997;38:296–302
28. Hendrick RE, Haacke EM. **Basic physics of MR contrast agents and maximization of image contrast.** *J Magn Reson Imaging* 1993;3:137–148
29. Pawlik G, Rackl A, Bing RJ. **Quantitative capillary topography and blood flow in the cerebral cortex of cats: an in vivo microscopic study.** *Brain Res* 1981;208:35–58
30. Malonek D, Grinvald A. **Interactions between electrical activity and cortical microcirculation revealed by imaging spectroscopy: Implications for functional brain mapping.** *Science* 1996; 272:551–554
31. Turner R, Grinvald A. **Direct visualization of patterns of deoxygenation and reoxygenation in monkey cortical vasculature during functional brain activation.** Thirteenth Annual Meeting of the Society of Magnetic Resonance 1994 S:430
32. Lee AT, Glover GH, Meyer CH. **Discrimination of large venous vessels in time-course spiral blood-oxygen-level-dependent magnetic resonance functional neuroimaging.** *Magn Reson Med* 1995;33:745–754
33. Erberich SG, Fellenberg M, Krings T, Kemeny S, Willmes K, Reith W. **Unsupervised time course analysis of functional magnetic resonance imaging (fMRI) using self-organizing maps (SOM).** *Proc SPIE Med Imag* 1999, in press
34. Brooks RA, Di Chiro G. **Magnetic resonance imaging of stationary blood: a review.** *Med Phys* 1987;14:903–913
35. Frahm J, Merboldt KD, Hänicke W. **Functional MRI of human brain activation at high spatial resolution.** *Magn Reson Med* 1993;29:139–144
36. Fisel CR, Ackerman JL, Buxton RB, et al. **MR contrast due to microscopically heterogeneous magnetic susceptibility: numerical simulations and applications to cerebral physiology.** *Magn Reson Med* 1991;17:336–347